Available online at http://scik.org
J. Math. Comput. Sci. 5 (2015), No. 4, 473-498
ISSN: 1927-5307

ANALYSIS OF THE CASSON FLUID MODEL FOR BLOOD FLOW THROUGH AN ARTERY WITH MILD STENOSIS

HAMED M. SAYED[1,3], EMAD H. ALY[2,3,*]

[1]Department of Mathematics, Faculty of Sciences and Arts, Taibah University, Yanbu, Saudi Arabia

[2]Department of Mathematics, Faculty of Science, University of Jeddah, Jeddah 21589, Saudi Arabia

[3]Department of Mathematics, Faculty of Education, Ain Shams University, Roxy 11757, Cairo, Egypt

Abstract. In this paper, flow of the blood through asymmetric artery with mild stenosis has been investigated. The effect of asymmetrical shape and non–Newtonian behaviour of blood, represented by Casson fluid, are simultaneously considered. The expressions for velocity, resistance impedance, wall shear stresses and wall apparent viscosity are computed. The graphical results have been examined for different values of the parameters involved on the problem. It was observed that the resistance impedance increases as the stenosis length, stenosis size and flow rate increase, and it decreases as the stenosis shape parameter and yield value increases. It has been shown that the axial velocity and the apparent viscosity give larger values in the upper–region as compared these values in the lower–region. Also, the apparent viscosity increases as stenosis size, stenosis shape parameters and yield value increase while it decreases when flow rate increases. Further, when stenosis shape parameter increases, there is a convergence at the curves of the wall shear stresses in the upper–region while these is divergence at them in the lower–region.

Keywords: Casson fluid; Non–Newtonian; Blood; Artery; Stenosis.

2010 AMS Subject Classification: 76A05.

*Corresponding author.

E-mail addresses: efarag@uj.kau.sa, emad-aly@hotmail.com

Received: March 12, 2015

1. Introduction

Blood is a concentrated suspension of formed cellular elements including red blood cells (RBCs or erythrocytes), white blood cells (WBCs or leukocytes) and platelets (thrombocytes). These cellular elements are suspended in an aqueous polymeric and ionic solution of flow viscosity, the plasma, containing electrolytes and organic molecules such as metabolites, hormones, enzymes, antibodies and other proteins. The formed elements are produced in the bone marrow and represent approximately 45% by volume of the normal blood [1].

Blood flow in the vascular system is complicated in many respects and thus simplifying assumptions are often made. Under normal condition, blood circulates within the body's vascular network. However, it has an inherent tendency to clot that is balanced by endothelium. The clot formulation occurs for various reasons, endothelial injury, endothelial dysfunction, or flow stagnation and recirculation among others. Clot formulation occurs when the initiating stimulus exceeds certain threshold. Clots are formed at end of a serious of interacting biochemical processes: platelet adhesion, activation and aggregation, coagulation, polymerization of fibrin monomers formed from fibrinogen, and cross liking of the fibrin polymers stands to form a fibrin network [2] and [3]. More applications can be found in [4], [5], [6], and [7].

The study of blood flow through stenosed arteries is very important because of the fact that the cause and development of many arterial diseases leading to the malfunction of the cardiovascular system are, to a great extent, related to flow characteristics of the blood. Among the various arterial diseases, the development of arteriosclerosis in blood vessels is quite common which may be attributed to accumulation of lipids in the arterial wall [8]. Arteries are narrowed by the development of atherosclerotic plaques that protrude into the lumen, resulting in stenosed arteries [9]. As an obstruction developed in an artery, one of the most serious consequences is the increased resistance and the associated reduction of blood flow to the particular vascular bed supplied by the artery [10]. There ia a strong evidence that hemodynamical factors such as separation, flow recirculation, low and oscillatory wall shear stress, play a major role in the development and progression of atherosclerotic plaques and other arterial lesions (e.g. [11] and [1]) but their role is not completely understood. Thus, the presence of stenosis can lead to serious circulatory disorder.

The assumption of Newtonian behaviour of blood is acceptable for high shear rate flow, e.g. in the case of flow through large arteries. However, it is not valid when the shear rate is low which is the case in small arteries and in the downstream side of the stenosis. The non–Newtonian character of blood is typical in small arteries and veins where the presence of the cells induces that specific behaviour [12].

Experiments on blood at low shear rates are extremely difficult to perform and consequently a controversy remains on the behaviour of blood at the limit of zero shear rate. Despite this controversy, it is commonly accepted that blood displays a yield stress, namely, there is a critical value of the yield stress below which blood does not flow. The treatment of the yield stress as a material parameter should be therefore independent of experimental factors and of yielding criteria but this is not the case of blood. In fact there exists a large variation in yield stress values for blood reported in the literature (e.g. [13]). The finite time required for the changes in blood microstructure is related to blood yield stress and thixotropy. Charm and Kurland [14] found that Casson model [15] gives the best fit to the blood data. Casson model is generalization of the Bingham model that can capture both the yield stress and the shear–thinning behaviour of blood.

In the past years, numerous researches of clinical and computational fluid dynamical analysis have been performed to investigate the flow phenomena in the human artery. Charkravarty et al. [16] presented a theoretical investigation to examine some of the significant characteristics of the two–layered non–Newtonian rheology of blood flowing through a tapered flexible artery in the presence of stenosis under pulsatile pressure gradient. Siddiqui *et al.* [17] studied the pulsatile flow of blood in a stenosed artery by modelling blood as a Casson fluid. Sarifuddin *et al.* [18] reviewed the mathematical model representing the dynamic response of heat and mass transfer to blood streaming through the arteries under stenotic condition, where the blood and arterial wall was treated as a generalized Newtonian fluid and a rigid having differently shaped stenoses, respectively. Javadzadegan *et al.* [19] simulated the behaviour of two mathematical models for blood as cross fluid and Oldroyed–B fluid in an artery with partial constriction. Sankar and Lee [20] studied the pulsatile flow of blood through mild stenoses artery, where the blood was treated as Herschel–Bulkely model.

Recently, Nadeem *et al.* [21] analyzed the blood flow through a tapered artery with mild stenosis. They assumed that the flow is steady and blood is treated as non–Newtonian power law fluid model. Bandyopadhyay and Layek [22] considered a simple two–dimensional planar geometrical model of a Newtonian viscous fluid through a constricted channel and the stream function vorticity approach has been adopted. Blood flow in arteries is mostly dominated by unsteady flow phenomena and the rigidity of the wall may be reasonably assumed. They mentioned in their study to understand the flow behaviour in pulsatile flows in a constricted channel. Very recently, Ellahi *et al.* [23] examined the unsteady and incompressible flow of nonNewtonian micropolar fluid through composite stenosis with sip velocity. Gupta and Gupta [24] gave a model to study the effects of axial variation of viscosity caused by accumulation of red cells in the stenosis region of an artery with mild stenosis on resistance to flow and wall shear stress. Awgichew *et al.* [25] studied the steady flow of an incompressible couple stress fluid in a two dimensional uniform channel with stenosis under the influence of a magnetic field. Nandakumar *et al.* [26] discussed the effects of percentage stenosis and Reynolds number on steady flow, and Womersley number on pulsatile flow, of blood (modeled as the shear thinning model proposed by Yeleswarapu) through a two dimensional channel with stenosis.

The purpose of this work is to mathematically simulate the behaviour of blood as Casson fluid in an asymmetric artery with mild stenoses. The arterial wall segment is considered rigid as well as deformable because, in the vicinity of the stenosis, it is usually relatively rigid when stenosis develop in the human vasculature. To neglect the entrance, end and special wall effects, the artery length is assumed to be large enough as compared to its width. The effects of asymmetric stenosis and non–Newtonian assumption of blood with various flow quantities are discussed. The current model can include the important geometrical features of stenosed arteries which may be useful to biomedical engineers in developing biomedical instruments for treatment (surgical) modalities. Review of the problem is accordance with the following: Section 2 contains the governing equations, motion and constitutive, for Casson fluid are modelled and non–dimensionalized. Exact solution of these equation, along with the boundary conditions of stenosed asymmetric artery, are resulted in Section 3. In Addition, the flow rate, resistance to flow, wall shear stresses and apparent viscosity at the walls are expressed in the this section.

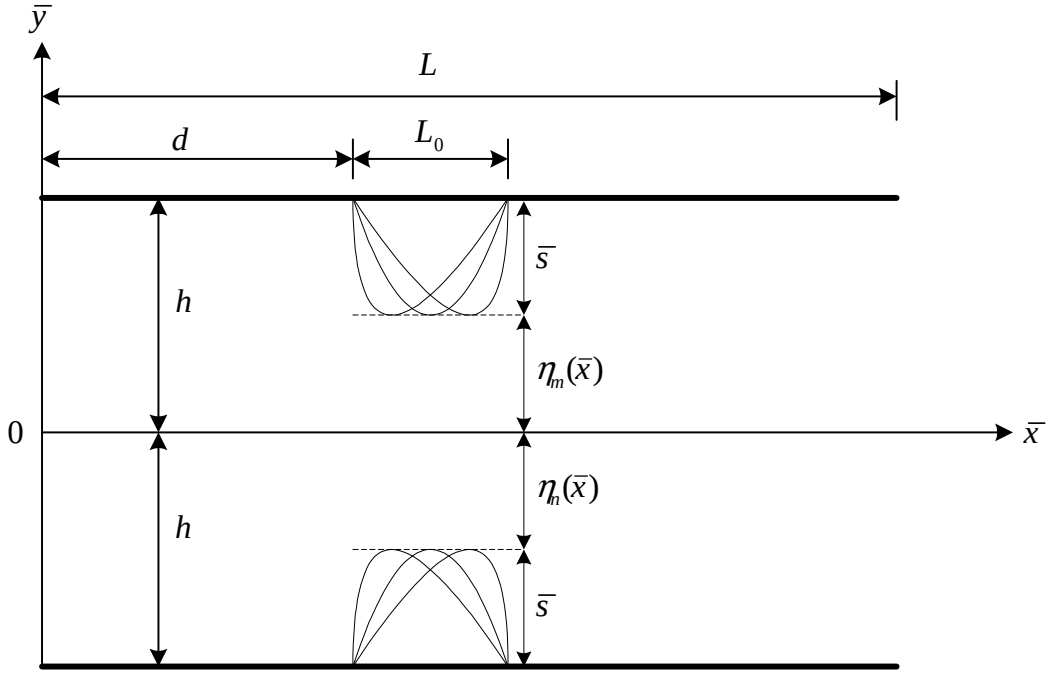

FIGURE 1. Schematic diagram of the mathematical model of the problem under investigation and the co–ordinate system employed.

The physical features of various emerging parameters are introduced and discussed, through the appropriate graphs, in Section 4. Conclusions are given in Section 5.

2. **Governing equations**

2.1. **Modelling of the problem.** The segment of the stenosed artery under consideration is simulated as a uniform rigid channel containing a non–Newtonian fluid representing the flowing blood. The flow is considered as unsteady and laminar with mild stenosis, where blood is treated as incompressible Casson fluid. To examine the effect of stenosis shape parameters, we consider blood flow through a longitudinally non–symmetrical, and transversally asymmetric stenosis, where there are two types of the shapes characterize the arterial segment which are often referred to as lower–region and upper–region; such that the shape of stenosis can be changed only by varying parameters n and m, respectively, as seen later. Fig. 1 shows the schematic of the investigated problem, where $\bar{x}-$ and $\bar{y}-$ coordinates are taken along the axis of the artery and normal to $\bar{x}$, respectively. The geometry of the channel upper walls is given by ([17], [27])

$$\bar{\eta}_m(\bar{x}) = \begin{cases} h - \bar{A}_m \left[L_0^{m-1}(\bar{x}-d) - (\bar{x}-d)^m \right], \text{ in } d \le \bar{x} \le d + L_0, \\ \\ h \qquad\qquad\qquad\qquad\qquad\qquad \text{otherwise}, \end{cases} \tag{1}$$

and of the lower wall by

$$\bar{\eta}_n(\bar{x}) = \begin{cases} -h + \bar{A}_n \left[L_0^{n-1}(\bar{x}-d) - (\bar{x}-d)^n \right], \text{ in } d \le \bar{x} \le d + L_0, \\ \\ -h \qquad\qquad\qquad\qquad\qquad\qquad \text{otherwise}, \end{cases} \tag{2}$$

where L_0 represents the length of the stenosis, d denotes its location, $\bar{\eta}_m(\bar{x})$ and $\bar{\eta}_n(\bar{x})$ are the upper and lower stenosis segments, respectively, $\bar{x}$ is along the axis of the artery and h is the maximum projection of the stenosis into the lumen. In addition, the parameters $\bar{A}_m$ and $\bar{A}_n$ are expressed as

$$\begin{cases} \bar{A}_m = \dfrac{\bar{s}}{h\, L_0^m}\, m^{\frac{m}{m-1}}, \\ \\ \bar{A}_n = \dfrac{\bar{s}}{h\, L_0^n}\, n^{\frac{n}{n-1}}, \end{cases} \tag{3}$$

where $\bar{s}$ denotes the maximum height of the stenosis at $\bar{x} = d + \frac{L_0}{m^{\frac{m}{m-1}}}$ and $\bar{x} = d + \frac{L_0}{n^{\frac{n}{n-1}}}$ for the upper and lower walls, respectively, such that $\frac{\bar{s}}{h} \ll 1$ (the mild stenosis case).

The equations governing the steady flow of an incompressible Casson fluid in the absence of body force are

$$\frac{\partial \bar{u}}{\partial \bar{x}} + \frac{\partial \bar{v}}{\partial \bar{y}} = 0, \tag{4}$$

$$\begin{cases} \rho \left(\bar{u}\, \dfrac{\partial \bar{u}}{\partial \bar{x}} + \bar{v}\, \dfrac{\partial \bar{u}}{\partial \bar{y}} \right) = -\dfrac{\partial \bar{P}}{\partial \bar{x}} + \dfrac{\partial \bar{\tau}_{xx}}{\partial \bar{x}} + \dfrac{\partial \bar{\tau}_{xy}}{\partial \bar{y}}, \\ \\ \rho \left(\bar{u}\, \dfrac{\partial \bar{v}}{\partial \bar{x}} + \bar{v}\, \dfrac{\partial \bar{v}}{\partial \bar{y}} \right) = -\dfrac{\partial \bar{P}}{\partial \bar{y}} + \dfrac{\partial \bar{\tau}_{yx}}{\partial \bar{x}} + \dfrac{\partial \bar{\tau}_{yy}}{\partial \bar{y}}, \end{cases} \tag{5}$$

where $(\bar{u}, \bar{v})$ are the velocity components in the $(\bar{x}, \bar{y})$ directions, respectively, ρ and $\bar{P}$ are the fluid density and pressure, respectively.

The constitutive equation for Casson fluid is given by [15],

$$|\bar{\tau}| = \left[\mu_0^{\frac{1}{2}} + \left(\frac{\bar{\tau}_0}{|\bar{\dot{\gamma}}|}\right)^{\frac{1}{2}}\right]^2 \bar{\dot{\gamma}} \qquad \text{at} \quad |\bar{\tau}| \geq |\bar{\tau}_0|, \tag{6}$$

$$\bar{\dot{\gamma}} = 0 \qquad \text{at} \quad |\bar{\tau}| \leq |\bar{\tau}_0|, \tag{7}$$

where $\bar{\tau}$ represents the shear stress, μ_0, $\bar{\dot{\gamma}}$ and $\bar{\tau}_0$ are the Casson viscosity, rate of strain component and yield value, respectively. For blood, $\bar{\tau}_0$ is related to the hematocrit as

$$\bar{\tau}_0^{\frac{1}{3}} = \frac{1}{100} B(H - H_m), \tag{8}$$

where $B = 0.0037 \pm 0.001 (\mathrm{N/m^2})^{\frac{1}{3}}$, where H is the normal hematocrit and H_m is the hematocrit below, in which there is no yield stress.

2.2. **Dimensionless formulation.** On introducing the following set of non-dimensional quantities

$$\begin{cases} x = \dfrac{\bar{x} - d}{L_0},\ y = \dfrac{\bar{y}}{h},\ u = \dfrac{\bar{u}}{U_0},\ v = \dfrac{L_0}{hU_0}\bar{v},\ P = \dfrac{h^2}{\mu_0 L_0 U_0}\bar{P},\ s = \dfrac{\bar{s}}{h}, \\ \\ \tau = \dfrac{h}{U_0\mu_0}\bar{\tau},\ \tau_0 = \dfrac{h}{U_0\mu_0}\bar{\tau}_0,\ \dot{\gamma} = \dfrac{h}{U_0}\bar{\dot{\gamma}}, \end{cases} \tag{9}$$

where U_0 is the maximum velocity of the blood at the entrance of the channel, Eqs. (1)–(7) can be therefore rewritten in the dimensionless form as follows

$$\eta_m(x) = \begin{cases} 1 - A_m \left[L_0^m (x - x^m)\right],\ 0 \leq x \leq 1, \\ \\ 1 \qquad\qquad\qquad\qquad \text{otherwise}, \end{cases} \tag{10}$$

$$\eta_n(x) = \begin{cases} -1 + A_n \left[L_0^n (x - x^n)\right],\ 0 \leq x \leq 1, \\ \\ -1 \qquad\qquad\qquad\qquad \text{otherwise}, \end{cases} \tag{11}$$

where

$$A_m = \frac{s}{h\, L_0^m}\, m^{\frac{m}{m-1}},\ \text{and}\ A_n = \frac{s}{h\, L_0^n}\, n^{\frac{n}{n-1}}, \tag{12}$$

$$\delta\left(\frac{\partial u}{\partial x}+\frac{\partial v}{\partial y}\right)=0, \tag{13}$$

$$\begin{cases} Re\ \delta\left(u\,\dfrac{\partial u}{\partial x}+v\,\dfrac{\partial u}{\partial y}\right)=-\dfrac{\partial P}{\partial x}+\delta\dfrac{\partial \tau_{xx}}{\partial x}+\dfrac{\partial \tau_{xy}}{\partial y}, \\ \\ Re\ \delta^3\left(u\,\dfrac{\partial v}{\partial x}+v\,\dfrac{\partial v}{\partial y}\right)=-\dfrac{\partial P}{\partial y}+\delta^2\dfrac{\partial \tau_{yx}}{\partial x}+\delta\dfrac{\partial \tau_{yy}}{\partial y}, \end{cases} \tag{14}$$

where $Re=\frac{\rho h U_0}{\mu_0}$ is the Reynold's number and $\delta=\frac{h}{L_0}$ is the geometric parameter where $(\delta \ll 1)$. Finally, Casson model in the dimensionless form is given by

$$|\tau|=\left[1+\left(\frac{\tau_0}{|\dot{\gamma}|,}\right)^{\frac{1}{2}}\right]^2\dot{\gamma} \qquad \text{at} \quad |\tau|\geq|\tau_0|, \tag{15}$$

$$\dot{\gamma}=0 \qquad \text{at} \quad |\tau|\leq|\tau_0|. \tag{16}$$

3. **Solution of the problem**

Solution of Eqs. (13) and (14) seems to be very difficult task due to the non–linearity terms, depending on the stenosis size [28]. However, certain terms in these equations are of less importance than others. Considering the case of mild stenosis, under the following conditions [29],

$$\frac{s}{h}\ll 1,\ Re\frac{s}{L_0}n^{\frac{1}{n-1}}\ll 1,\ Re\frac{s}{L_0}m^{\frac{1}{m-1}}\ll 1,\ \frac{h}{L_0}n^{\frac{1}{n-1}}\sim O(1),\ \frac{h}{L_0}m^{\frac{1}{m-1}}\sim O(1), \tag{17}$$

these equations can be therefore simplified to

$$\frac{\partial P}{\partial x}+\frac{\partial \tau_{xy}}{\partial y}=0, \tag{18}$$

$$\frac{\partial P}{\partial y}=0, \tag{19}$$

where the shear stress $\tau=-\tau_{xy}$, which under the condition that $\tau_{xy}=0$ at $y=0$, is given by

$$\tau_{xy}=-\frac{\partial P}{\partial x}\,y. \tag{20}$$

It should be also noted that the continuity equation is identically satisfied since the flow is one-dimensional and fully developed.

When shear stress and strain rate have opposite signs at $|\tau| \geq \tau_0$, Eq. (6) can be written as, for $\frac{\partial u}{\partial y} < 0$, $\tau_{xy} > 0$ and $0 \leq y \leq \eta_m$,

$$\tau_{xy} = \tau_0 + \left(-\frac{\partial u}{\partial y}\right) + 2\ \tau_0^{\frac{1}{2}}\ \left(-\frac{\partial u}{\partial y}\right)^{\frac{1}{2}}, \tag{21}$$

and as, for $\frac{\partial u}{\partial y} > 0$, $\tau_{xy} < 0$ and $\eta_n \leq y \leq 0$,

$$\tau_{xy} = -\left(\tau_0 + \frac{\partial u}{\partial y} + 2\ \tau_0^{\frac{1}{2}}\ \left(\frac{\partial u}{\partial y}\right)^{\frac{1}{2}}\right). \tag{22}$$

However, for $|\tau| \leq \tau_0$ and $\eta_{cn} \leq y \leq \eta_{cm}$, Eq. (7) is written as

$$\dot{\gamma}_{xy} = 0. \tag{23}$$

On substituting Eq. (21) on Eq. (20) and integrating the resulting equation, we get

$$\frac{\partial P}{\partial x} = -\frac{\partial}{\partial y}\left[\tau_0 + \left(-\frac{\partial u}{\partial y}\right) + 2\ \tau_0^{\frac{1}{2}}\ \left(-\frac{\partial u}{\partial y}\right)^{\frac{1}{2}}\right]. \tag{24}$$

On setting $-\frac{\partial u}{\partial y} = \Phi^2$, this results

$$\Phi^2 + 2\ \tau_0^{\frac{1}{2}}\Phi + \tau_0 + \frac{\partial P}{\partial x}y = 0, \tag{25}$$

whose roots are given by

$$\Phi = \frac{1}{2}\left[-2\ \tau_0^{\frac{1}{2}} \pm y^{\frac{1}{2}}\ (-4P_{,x})^{\frac{1}{2}}\right], \tag{26}$$

On using Eq. (26), we get

$$\frac{\partial u}{\partial y} = -\frac{1}{4}\left[4\tau_0 \mp 2\ \tau_0^{\frac{1}{2}}\ (-4P_{,x})^{\frac{1}{2}}\ y^{\frac{1}{2}} + (-4P_{,x})\ y\right]. \tag{27}$$

Integration Eq. (27) and using the condition that $u = 0$ at $y = \eta_n$, we obtain

$$u = \frac{1}{4}\left[4\tau_0(\eta_m - y) \pm \frac{4}{3}\ \tau_0^{\frac{1}{2}}\ (4P_{,x})^{\frac{1}{2}}\left((-\eta_m)^{\frac{3}{2}} - (-y)^{\frac{3}{2}}\right) - \frac{1}{2}\ (4P_{,x})\left(\eta_m^2 - y^2\right)\right]. \tag{28}$$

Similarity, on solving Eq. (20) by using Eq. (22), we get

$$\frac{\partial P}{\partial x} = \frac{\partial}{\partial y}\left(\frac{\partial u}{\partial y} + \tau_0 + 2\tau_0^{\frac{1}{2}}\left(\frac{\partial u}{\partial y}\right)^{\frac{1}{2}}\right). \tag{29}$$

By integration and setting $\frac{\partial u}{\partial y} = \Psi^2$, it results

$$\Psi^2 + 2\ \tau_0^{\frac{1}{2}}\Psi + \tau_0 - \frac{\partial P}{\partial x}y = 0, \tag{30}$$

whose roots are given by

$$\Psi = \frac{1}{2}\left[-2\ \tau_0^{\frac{1}{2}} \pm (-4P_{,x})^{\frac{1}{2}}\, y^{\frac{1}{2}}\right], \tag{31}$$

On using Eq. (31), we get

$$\frac{\partial u}{\partial y} = \frac{1}{4}\left[4\tau_0 \mp 2\ \tau_0^{\frac{1}{2}}\,(4P_{,x})^{\frac{1}{2}}\, y^{\frac{1}{2}} + (4P_{,x})\, y\right]. \tag{32}$$

Integration Eq. (32) and using the condition that $u = 0$ at $y = \eta_m$, we get

$$u = -\frac{1}{4}\left[4\tau_0(\eta_n - y) \mp \frac{4}{3}\ \tau_0^{\frac{1}{2}}\,(4P_{,x})^{\frac{1}{2}}\left(\eta_n^{\frac{3}{2}} - y^{\frac{3}{2}}\right) + \frac{1}{2}\,(4P_{,x})\left(\eta_n^2 - y^2\right)\right]. \tag{33}$$

The upper limit of the plug flow region is obtained by

$$\eta_{cm} = \frac{\tau_0}{-P_{,x}}. \tag{34}$$

On using the condition $\tau_{yx} = \tau_c$ at $y = \eta_m$ [30] in Eq. (20), it results

$$\eta_m = \frac{\tau_c}{-P_{,x}}. \tag{35}$$

This leads that

$$\eta_{cm} = \tau\ \eta_m;\ 0 < \tau < 1, \tag{36}$$

where $\tau = \frac{\tau_0}{\tau_c}$. Similarity, the lower limit of the plug flow region can be obtained under the condition $\tau_{yx} = -\tau_c$ at $y = \eta_m$ as follows

$$\eta_{cn} = \tau\ \eta_n;\ 0 < \tau < 1. \tag{37}$$

On using relations (36) and (37) and taking $y = \eta_{cm}$ and η_{cn} in Eqs. (28) and (33), respectively, we get the plug velocities as

$$u_m = \frac{1}{4}\left[4\tau_0\left(\eta_m - \eta_{cm}\right) \pm \frac{4}{3}\,\tau_0^{\frac{1}{2}}\left(4P_{,x}\right)^{\frac{1}{2}}\left(\left(-\eta_m\right)^{\frac{3}{2}} - \left(-\eta_{cm}\right)^{\frac{3}{2}}\right) - \frac{1}{2}\left(4P_{,x}\right)\left(\eta_m^2 - \eta_{cm}^2\right)\right]. \tag{38}$$

$$u_n = -\frac{1}{4}\left[4\tau_0\left(\eta_n - \eta_{cn}\right) \mp \frac{4}{3}\,\tau_0^{\frac{1}{2}}\left(4P_{,x}\right)^{\frac{1}{2}}\left(\eta_n^{\frac{3}{2}} - \eta_{cn}^{\frac{3}{2}}\right) + \frac{1}{2}\left(4P_{,x}\right)\left(\eta_n^2 - \eta_{cn}^2\right)\right]. \tag{39}$$

3.1. **Flow rate.** We can define the dimensional flow rate $\bar{Q}$ by

$$\bar{Q} = \int_{\bar{\eta}_n}^{\bar{\eta}_m} \bar{u}\, d\bar{y}. \tag{40}$$

On using Eqs. (9), defining the dimensionless flow Q as $Q = \frac{\bar{Q}}{U_0 h}$ and substituting Eqs. (28), (33), (38) and (39) into Eq. (40), it may be then written as

$$Q = \int_{\eta_n}^{\eta_m} u\, dy = \int_{\eta_n}^{\eta_{cn}} u\, dy + \int_{\eta_{cn}}^{0} u_n\, dy + \int_{0}^{\eta_{cm}} u_m\, dy + \int_{\eta_{cm}}^{\eta_m} u\, dy, \tag{41}$$

which leads to

$$E_1\,\xi^2 \mp E_2\,\xi + E_3 = 0 \tag{42}$$

whose solution is given by

$$\xi = \frac{1}{2E_1}\left[\pm E_2 \pm \sqrt{E_2^2 - 4E_1E_3}\right], \tag{43}$$

where

$$\begin{cases} \xi^2 = 4P_{,x} \equiv F(\eta_m(x), \eta_n(x), Q), \\ E_1 = \frac{1}{3}\left(\eta_{cn}^3 - \eta_n^3 - \eta_{cm}^3 + \eta_m^3\right), \\ E_2 = \frac{4}{5}\tau_0^{\frac{1}{2}}\left(\eta_{cn}^{5/2} - \eta_n^{5/2} + \left(-\eta_{cm}\right)^{5/2} - \left(-\eta_m\right)^{5/2}\right), \\ E_3 = 2\tau_0\left(\eta_{cn}^2 - \eta_n^2 + \eta_{cm}^2 - \eta_m^2\right) + 4Q, \end{cases} \tag{44}$$

When $\eta_m = 1,\ \eta_n = -1,\ \eta_{cn} = -\tau,\ \eta_{cm} = \tau$, it results that

$$\begin{cases} E_1 = -\dfrac{2}{3}\left(\tau^3 + 1\right), \\ \\ E_2 = \dfrac{8}{5}\ \tau_0^{\frac{1}{2}}\left((-\tau)^{5/2} - (-1)^{5/2}\right), \\ \\ E_3 = 4\left(\tau_0(\tau^2 - 1) + Q\right). \end{cases} \tag{45}$$

3.2. **Resistance impedance.** The pressure drop $\Delta P (= P_0$ at $x = 0,\ P_L$ at $x = L)$ across the stenosis between the sections $x = 0$ and $x = L$ is resulted from Eq. (44–1), as in [31], by

$$\Delta P = \int_0^L \frac{dP}{dx}\, dx. \tag{46}$$

The dimensionless resistance to the flow (or the resistance impedance) is denoted by λ and defined as

$$\lambda = \frac{P_L - P_0}{Q} = \frac{1}{Q}\left[\int_0^d + \int_d^{d+\frac{L_0}{L}} + \int_{d+\frac{L_0}{L}}^1\right]\xi^2 dx. \tag{47}$$

Since $\eta_m(x) = 1$ and $\eta_n(x) = -1$ in the regions $0 \le x \le d$ and $d + \frac{L_0}{L} \le x \le 1$, respectively, the resistance to the flow can be then simplified to

$$\lambda = \frac{1}{Q}\left(1 - \frac{L_0}{L}\right)\ \xi^2 \Bigg|_{\left\{\begin{array}{l} \eta_m(x) = 1 \\ \eta_n(x) = -1 \end{array}\right\}} + \frac{L_0}{QL}\int_0^1 \xi^2 dx. \tag{48}$$

3.3. **Expression for the wall shear stress.** The shearing stresses and (21) and (22) at the walls η_m and η_n are obtained, respectively, as

$$\tau_{xy} = \begin{cases} \left[\left(-\dfrac{\partial u}{\partial y}\right) + 2\tau_0^{\frac{1}{2}}\left(-\dfrac{\partial u}{\partial y}\right)^{\frac{1}{2}} + \tau_0\right] & \text{at} \quad y = \eta_m, \\ \\ -\left[\left(\dfrac{\partial u}{\partial y}\right) + 2\tau_0^{\frac{1}{2}}\left(\dfrac{\partial u}{\partial y}\right)^{\frac{1}{2}} + \tau_0\right] & \text{at} \quad y = \eta_n, \end{cases} \tag{49}$$

where

$$\frac{\partial u}{\partial y} = \begin{cases} -\frac{1}{4}\left[2\tau_0^{\frac{1}{2}} \pm \left(-4\eta_m\,\xi^2\right)^{\frac{1}{2}}\right]^2 & \text{at} \quad y = \eta_m, \\ \\ \frac{1}{4}\left[-2\tau_0^{\frac{1}{2}} \pm \left(4\eta_n\,\xi^2\right)^{\frac{1}{2}}\right]^2 & \text{at} \quad y = \eta_n. \end{cases} \tag{50}$$

3.4. **Apparent viscosity at the wall.** From Eqs. (6) and (7), the apparent viscosity $|\bar{\mu}| = \left[\mu_0^{\frac{1}{2}} + \bar{\tau}_0^{\frac{1}{2}}|\bar{\dot{\gamma}}|^{\left(-\frac{1}{2}\right)}\right]^2$ in the dimensionless form is given by [32]

$$|\mu| = \frac{|\bar{\mu}|}{\mu_0} = \left[1 + \tau_0^{\frac{1}{2}}|\dot{\gamma}|^{\left(-\frac{1}{2}\right)}\right]^2. \tag{51}$$

The apparent viscosity at the walls can be then expressed as follows

$$\mu = \begin{cases} \left[1 + \tau_0^{\frac{1}{2}}\left(-\frac{\partial u}{\partial y}\right)^{\left(-\frac{1}{2}\right)}\right]^2 & \text{at} \quad y = \eta_m, \\ \\ \left[1 + \tau_0^{\frac{1}{2}}\left(\frac{\partial u}{\partial y}\right)^{\left(-\frac{1}{2}\right)}\right]^2 & \text{at} \quad y = \eta_n, \end{cases} \tag{52}$$

where $\frac{\partial u}{\partial y}$ is defined in Eq. (50).

4. **Results and discussion**

To investigate the quantitative effects of $n, m, s/h, \tau_0$ and Q, MATHEMATICA 6 has been used to develop codes for numerical evaluations of the analytic results obtained for the axial velocity u, resistance to flow λ, wall shear stresses τ_{xy} and wall apparent viscosities μ, Eqs. (28), (33), (48), (49) and (52), respectively. Fig. 2 shows variation of the resistance to flow, λ, with stenosis length L_0/L. It may be observed that λ increases steeply as L_0/L increases and decreases as stenosis shape parameters m, n and $m = n$ increase. In addition, it increases when the stenosis size s/h increases. Further, we notice that λ sharply decreases as τ_0 increases, while it increases when Q increases.

Fig. 3 describes variation of λ with stenosis size s/h. It depicts that λ behaves in a completely similar manner as discussed for Fig. 2.

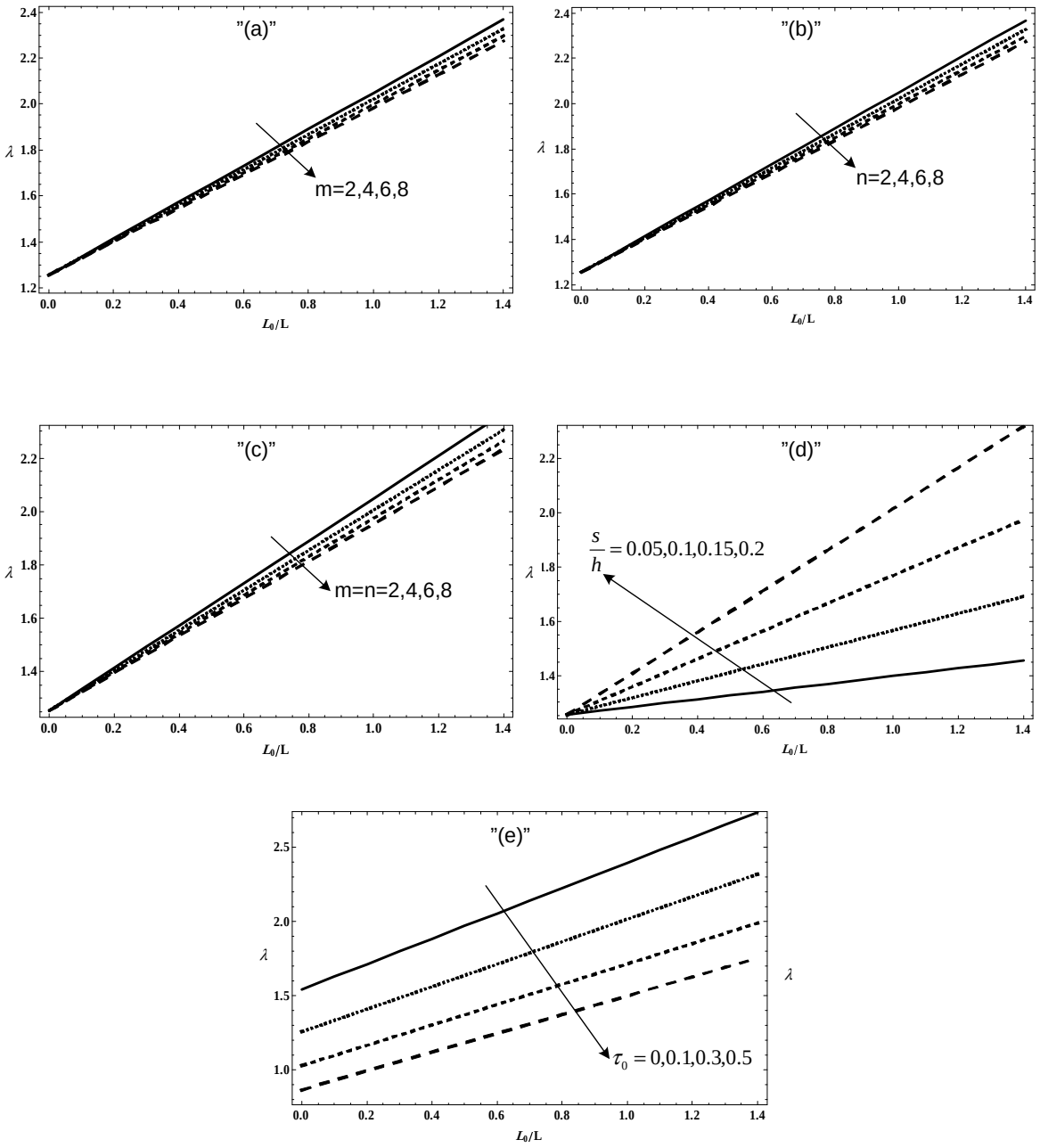

FIGURE 2. Variation of λ, the resistance to flow, with L_0/L, the stenosis length, at $\tau = 0.3$ for (a) $n = 2$, $\tau_0 = 0.1$, $Q = 3$, $s = 0.2h$, (b) $m = 2$, $\tau_0 = 0.1$, $Q = 3$, $s = 0.2h$, (c) $\tau_0 = 0.1$, $Q = 3$, $s = 0.2h$, (d) $m = 4$, $n = 3$, $\tau_0 = 0.1$, $Q = 3$, (e) $m = 4$, $n = 3$, $Q = 3$, $s = 0.2h$, and (f) $m = 4$, $n = 3$, $\tau_0 = 0.1$, $s = 0.2h$.

In Fig. 4, variation of the axial velocity, u, is studied as a function of the normal distance, y, for various values of the fluid, stenosis size, and stenosis shape parameters. It can be noted from Fig. 4(a) that for y in the range η_n and 0 with an increase in m, the velocity profile decreases (i.e., the curves representing the axial flow velocity do shift towards the origin with an increase

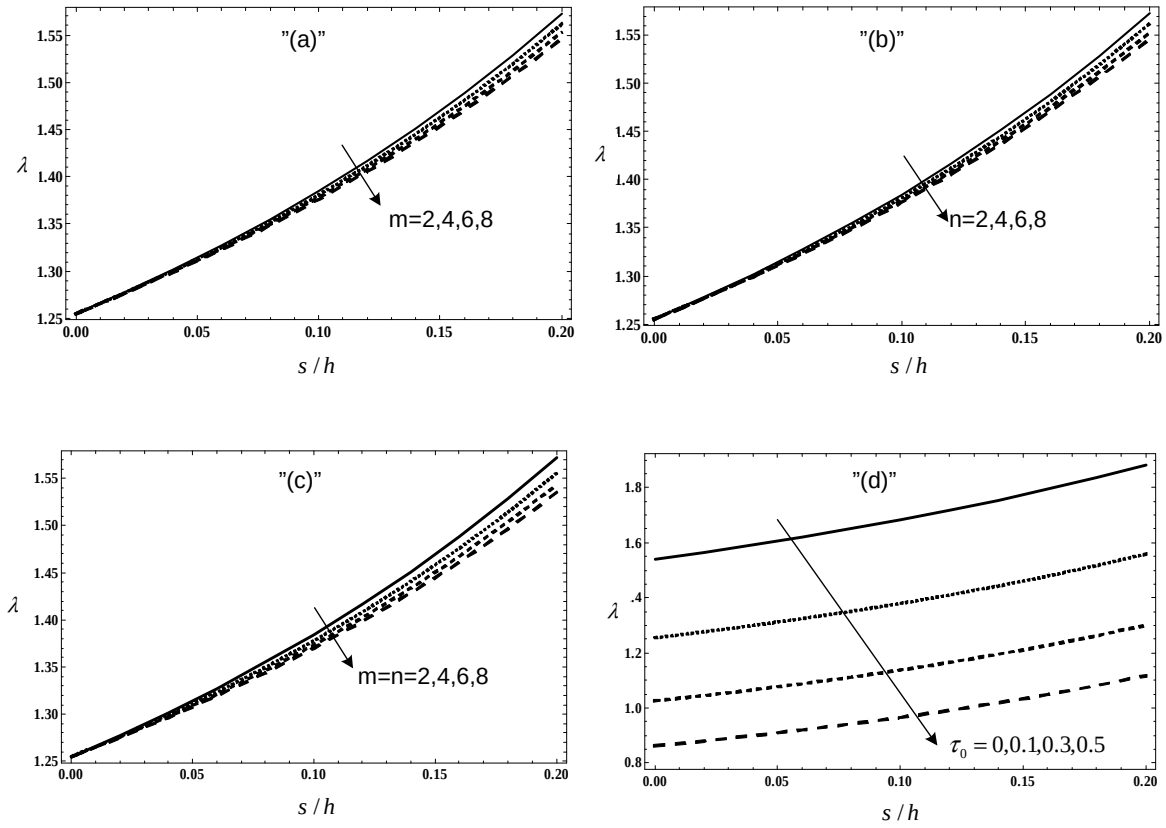

FIGURE 3. Variation of λ with s/h, the stenosis size, at $L_0 = 0.4L$ and $\tau = 0.3$ for (a) $n = 2$, $\tau_0 = 0.1$, $Q = 3$, (b) $m = 2$, $\tau_0 = 0.1$, $Q = 3$, (c) $\tau_0 = 0.1$, $Q = 3$, (d) $m = 4$, $n = 3$, $Q = 3$, and (e) $m = 4$, $n = 3$, $\tau_0 = 0.1$.

in m) while they shift away from the origin with an increase in m for y in the range 0 and η_m. Fig. 4(b) depicts that the velocity profile has an opposite behaviour as compared with that in Fig. 4(a). Moreover, in Fig. 4(c) as symmetric stenosis case (i.e. $m = n$) and for $y < -0.5$ and $y > 0.5$, the velocity increases with increasing values of stenosis shape parameter whereas it decreases with increasing values of stenosis shape parameter for y in the range -0.5 to 0.5. Fig. 4(d, e, f) show the variation of the axial velocity along the normal distance for different values of s/h, τ_0 and Q. It is found that with an increase of these parameters, the velocity profile increases. It is also seen that for $0 < y < \eta_m$, the axial velocity gives larger values as compared these values for $\eta_n < y < 0$ because the stenosis shape parameter m is higher in the former than that the stenosis shape parameter n.

Fig. 5(a) represents the variation of axial velocity with axial distance x for different values of m. It is evident from the graph that the axial velocity, u, steeply increases in the upstream from its approached value (i.e., at $x = 0$) to the peak value of the throat, then decreases in

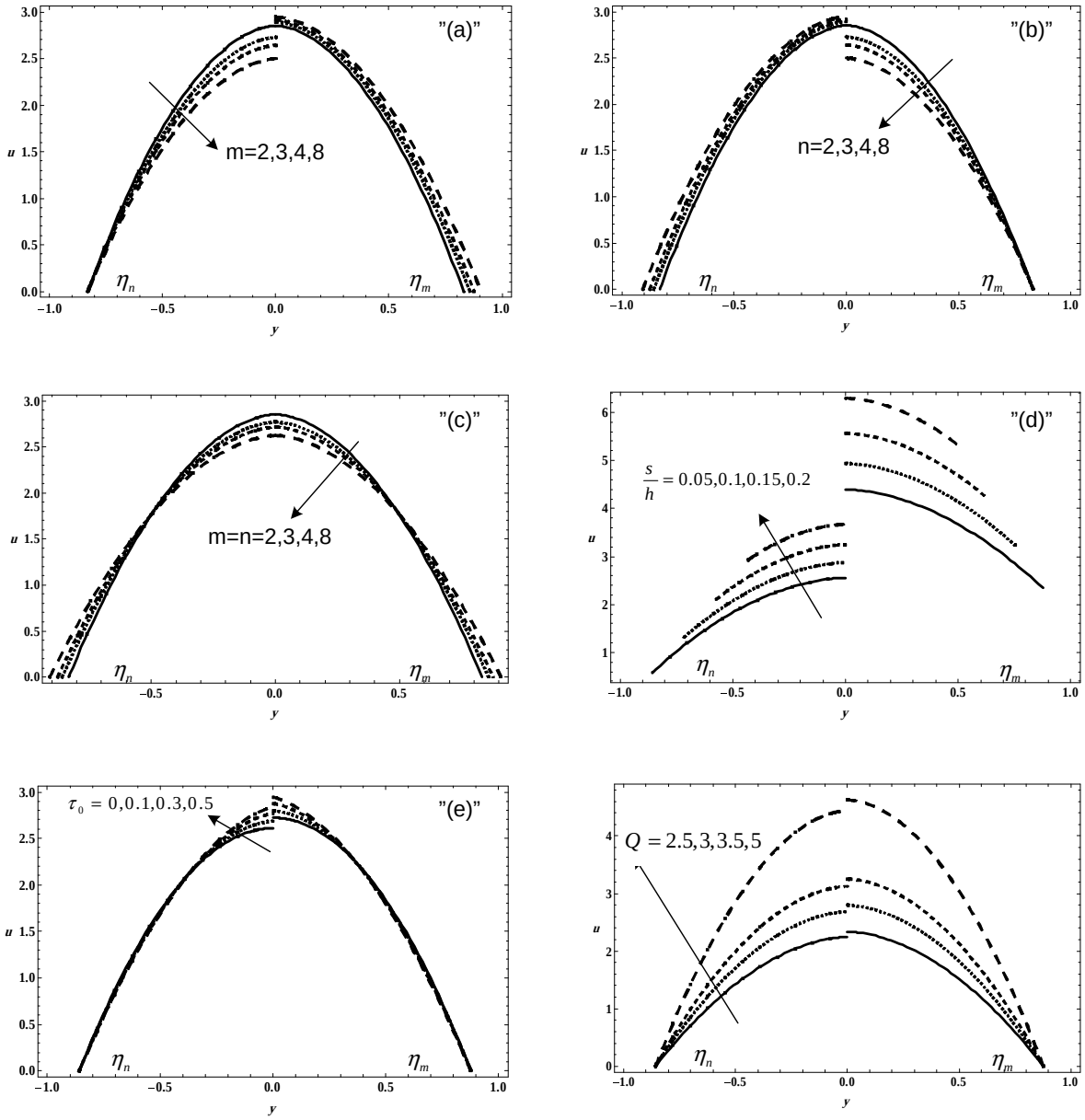

FIGURE 4. Variation of u, the axial velocity, with y for $\tau = 0.3$ and $x = 0.3$ at (a) $n = 2$, $\tau_0 = 0.1$, $Q = 3$, $s = 0.2h$, (b) $m = 2$, $\tau_0 = 0.1$, $Q = 3$, $s = 0.2h$, (c) $\tau_0 = 0.1$, $Q = 3$, $s = 0.2h$, (d) $m = 4$, $n = 3$, $\tau_0 = 0.1$, $Q = 3$, (e) $m = 4$, $n = 3$, $Q = 3$, $s = 0.2h$, and (f) $m = 4$, $n = 3$, $\tau_0 = 0.1$, $s = 0.2h$.

the downstream of the throat and assumes its approached magnitude at the endpoint of the constriction profile (i.e., at $x = 1$). The increasing rate of u (with respect to the axial distance) for $\eta_n < y < 0$ in the upstream of the throat decreases with the increasing values of m, whereas this rate in the downstream of the throat increases with m. It is also observed that this result is therefore a reversal behaviour with the observation of the axial velocity profile for $0 < y < \eta_m$. Fig. 5(b) and 5(c) show the influence of n and $(m = n)$, respectively, on the axial velocity profile.

It is observed that the opposite behaviour, of that described for the axial velocity in Fig. 5(a), occurs. In Fig. 5(d) we notice that with an increase stenosis size, s/h, axial velocity decreases. It is also seen that for the upper–region, $0 < y < \eta_m$, velocity gives larger values as compared to the lower–region, $\eta_n < y < 0$. Figs. 5(e) and 5(f) are prepared to see the variation of the axial velocity with τ_0 and Q. It is analyzed that with an increase in them, velocity profile increases. Also, as τ_0 and Q increase, the axial position of the throat approaches to the endpoint of the constriction profile and due to the rapid fall in the velocity profile from its peak value at the throat to approached value, one may anticipate the formulation of wake in the downstream of the throat.

In Fig. 6 we depict the variation of dimensionless apparent viscosity, μ, at the walls, with axial distance for various values of m, n, s/h, τ_0 and Q. It is found that the apparent viscosity steeply decreases in the upstream from its approached value (i.e., at $x = 0$) to the peak value at the throat and assumes its approached magnitude at the endpoint of the constriction profile (i.e., at $x = 1$). In addition, we observed that the values of μ, which appears in the lower–region, $\eta_n < y < 0$, are to be smaller than those in the upper–region, $0 < y < \eta_m$.

Fig. 7 describes variation of μ with the stenosis sizes s/h for different values of m, n, τ_0 and Q. In these graphs μ increases as s/h, m, n and τ_0 increase while it decreases when Q increases. In addition, for various values of n, m, $m = n$, τ_0 and Q, the apparent viscosity gives highly value in the upper–region than its value in the lower–region.

Fig. 8 illustrates variation of the wall shear stresses (WSS), τ_{xy}, for different values of n, m, s/h, τ_0 and Q. It can be noted that in the lower–region, τ_{xy} decreases with the axial distance, x, in the upstream of the stenosis throat and attains its maximum magnitude at the throat. It then increases in the downstream of the throat and achieves the same magnitude at the end point of the constriction profile (i.e., $x = 1$) same as its approached value at (i.e., $x = 0$) for any given set of parameters. Whereas in the upper–region, WSS follows the opposite tend as discussed above in the lower–region, except that the curves representing the wall shear stresses converge to each other in this region. The flow characteristic, τ_{xy}, decreases with increasing in the upstream of the throat but this property reverse in the downstream. However, we find that when $n = m$, the wall shear stresses follows the same tend as described for different values of m except the curves

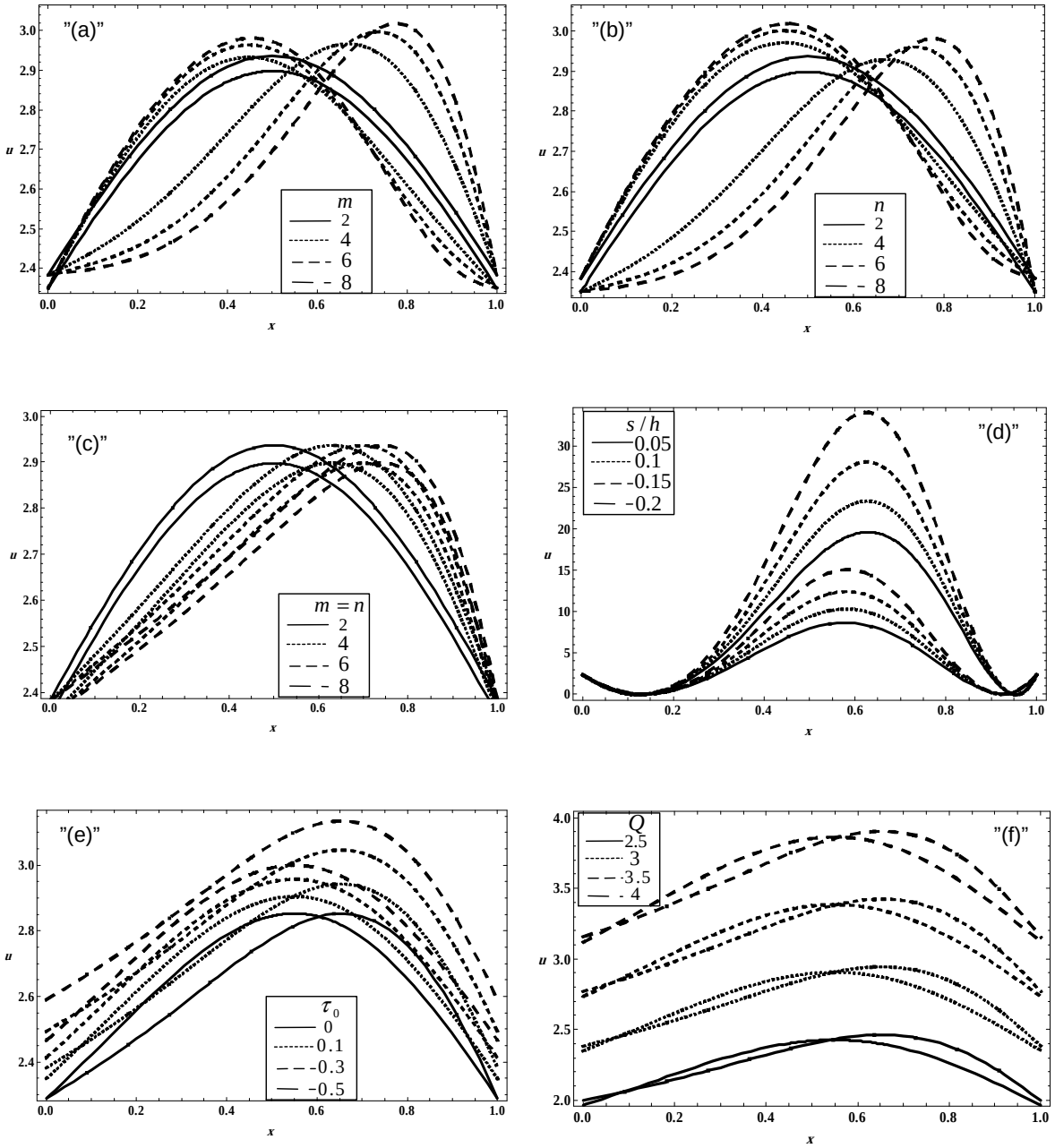

FIGURE 5. Variation of u with x at $\tau = 0.3$ and $y = 0.5$ for (a) $n = 2$, $\tau_0 = 0.1$, $Q = 3$, $s = 0.2h$, (b) $m = 2$, $\tau_0 = 0.1$, $Q = 3$, $s = 0.2h$, (c) $\tau_0 = 0.1$, $Q = 3$, $s = 0.2h$, (d) $m = 4$, $n = 3$, $\tau_0 = 0.1$, $Q = 3$, (e) $m = 4$, $n = 3$, $Q = 3$, $s = 0.2h$, and (f) $m = 4$, $n = 3$, $\tau_0 = 0.1$, $s = 0.2h$.

representing the wall shear stresses which behave the same manner in both regions. It is also observed that for different values of n, the wall shear stresses profile have the same behaviour when compared to the wall shear stresses profile as described in Fig. 8(a), except the curves of WSS are more closely values in the lower–region than in the upper–region. In addition, WSS increases as s/h and Q increase in the upper–region whereas it decreases in the lower–region.

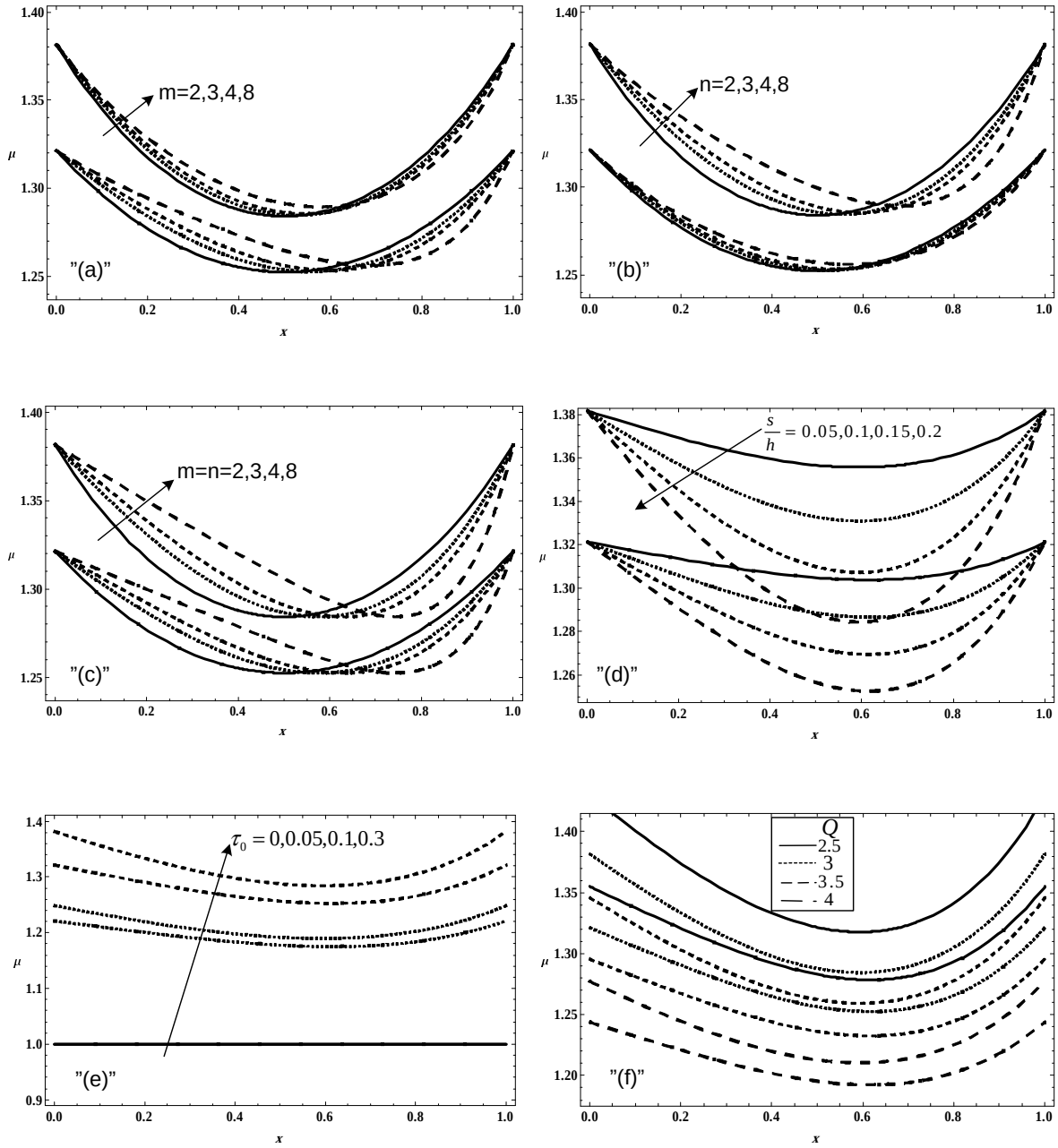

FIGURE 6. Variation of μ, the apparent viscosity, with x at $\tau = 0.3$ for (a) $n = 2$, $\tau_0 = 0.1$, $Q = 3$, $s = 0.2h$, (b) $m = 2$, $\tau_0 = 0.1$, $Q = 3$, $s = 0.2h$, (c) $\tau_0 = 0.1$, $Q = 3$, $s = 0.2h$, (d) $m = 4$, $n = 3$, $\tau_0 = 0.1$, $Q = 3$, (e) $m = 4$, $n = 3$, $Q = 3$, $s = 0.2h$, and (f) $m = 4$, $n = 3$, $\tau_0 = 0.1$, $s = 0.2h$.

It is also observed that for different values of τ_0, the influence on τ_{xy} matches the effect of each s/h and Q, except that in the upper–region the curves representing the wall shear stresses are identical as τ_0 increases. Moreover, it may be noted that WSS profiles have positive values in the upper–region while these profiles give negative values in the lower–region.

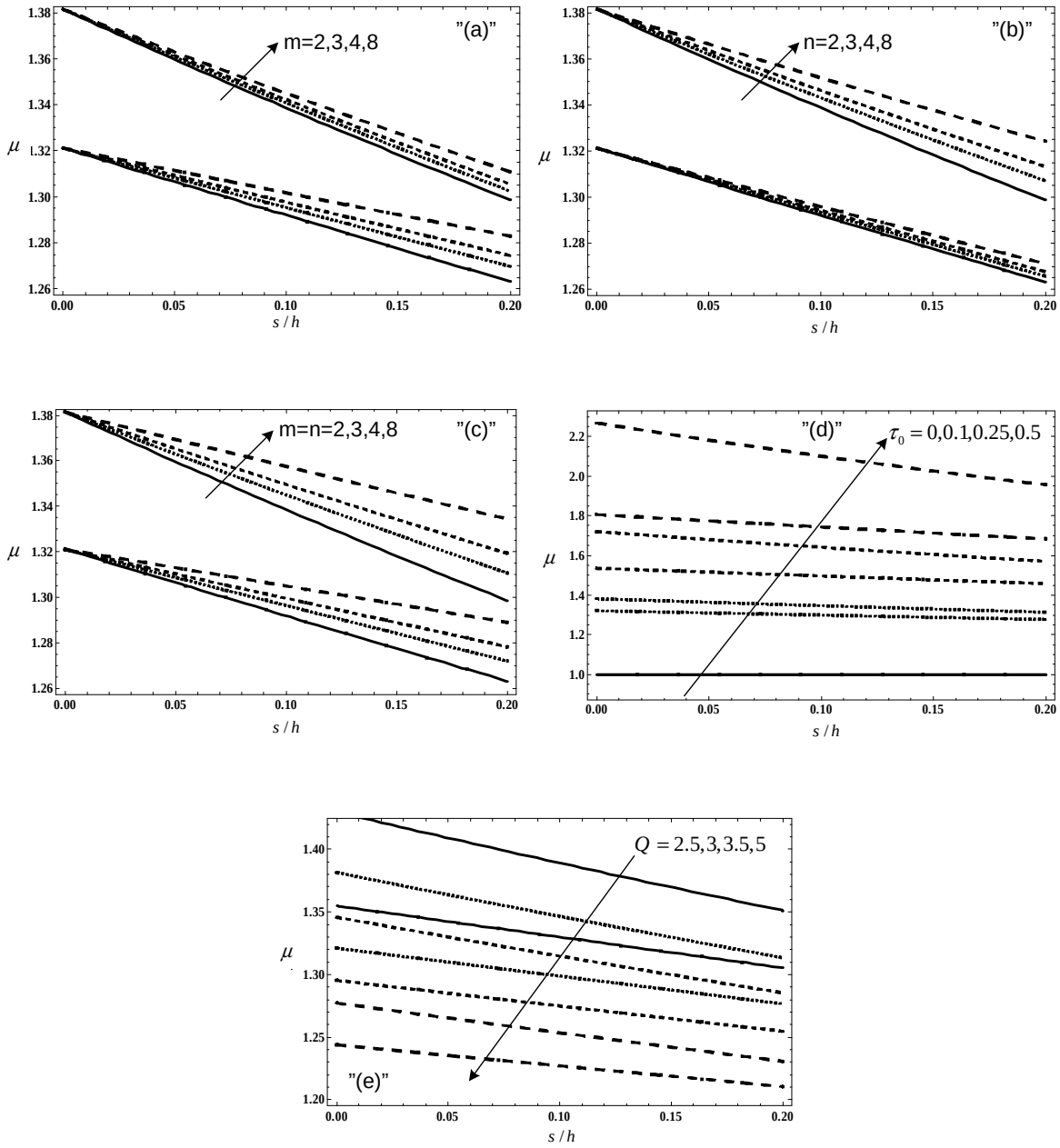

FIGURE 7. Variation of μ with s/h at $x = 0.3$ and $\tau = 0.3$ for (a) $n = 2$, $\tau_0 = 0.1$, $Q = 3$, (b) $m = 2$, $\tau_0 = 0.1$, $Q = 3$, (c) $\tau_0 = 0.1$, $Q = 3$, (d) $m = 4$, $n = 3$, $Q = 3$, and (e) $m = 4$, $n = 3$, $\tau_0 = 0.1$.

Fig. 9 reveals WSS, τ_{xy}, with stenosis size s/h for different values of n, m, τ_0 and Q. It depicts that in the upper–region τ_{xy} increases with increasing s/h and WSS attains its maximum magnitude at the stenosis throat. Whereas, in the lower–region the curves representing WSS is opposite like that was described previously. In addition, when m increases there is a convergence at the curves in the upper–region while there is divergence at them in the lower–region.

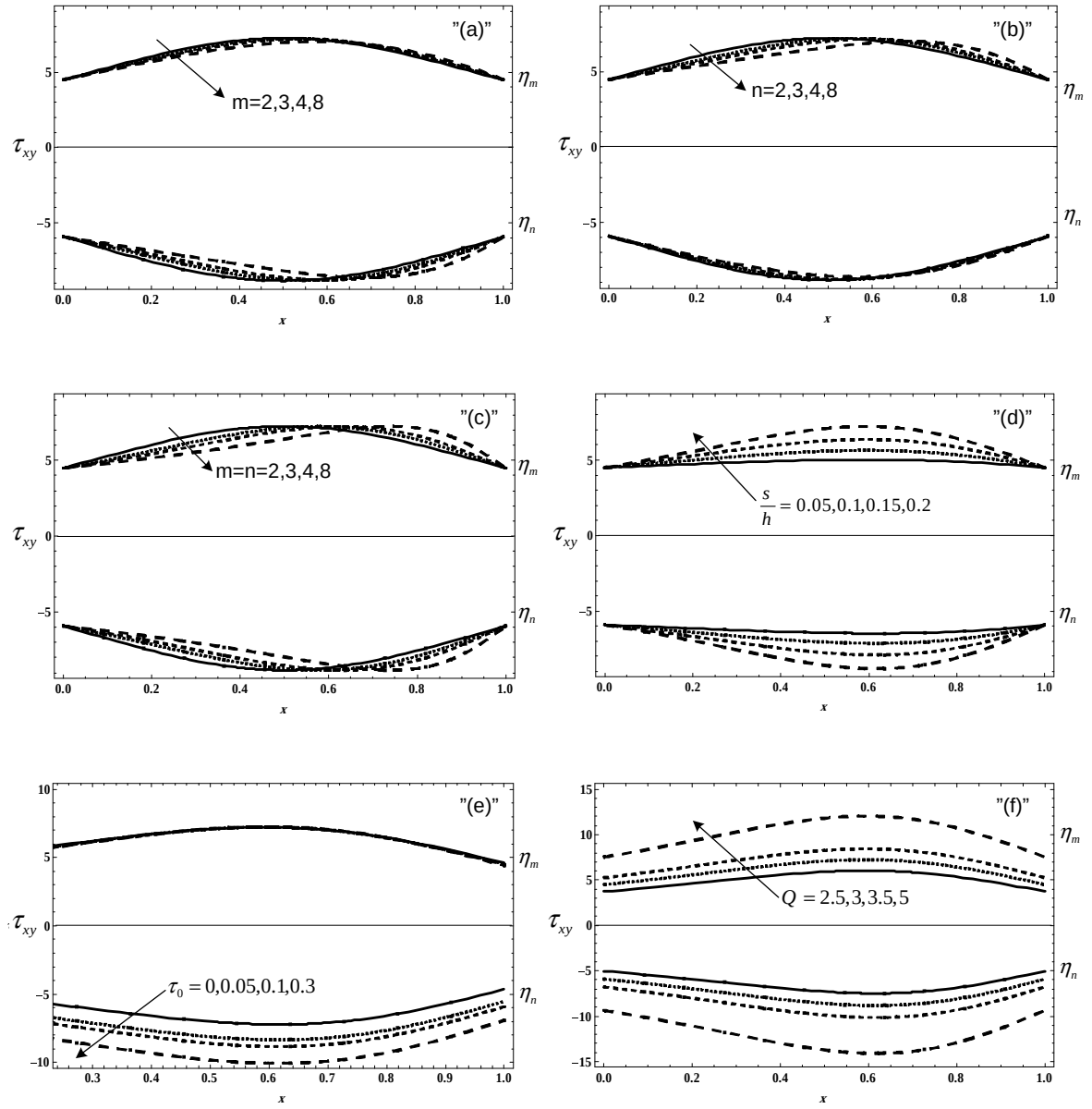

FIGURE 8. Variation of τ_{xy}, the wall shear stresses, with x at $\tau = 0.3$ for (a) $n = 2,\ \tau_0 = 0.1,\ Q = 3,\ s = 0.2h$, (b) $m = 2,\ \tau_0 = 0.1,\ Q = 3,\ s = 0.2h$, (c) $\tau_0 = 0.1,\ Q = 3,\ s = 0.2h$, (d) $m = 4,\ n = 3,\ \tau_0 = 0.1,\ Q = 3$, (e) $m = 4,\ n = 3,\ Q = 3,\ s = 0.2h$, and (f) $m = 4,\ n = 3,\ \tau_0 = 0.1,\ s = 0.2h$.

Moreover, the opposite happens when increasing n while it occurs similarity as $n = m$. Furthermore, in the upper–region when τ_0 and Q increase there is a substantial increase in WSS but decreases in the lower–region. It is also seen that the curves diverge gradually as τ_0 and Q increase, except that they are identical in the upper–region as τ_0 increases.

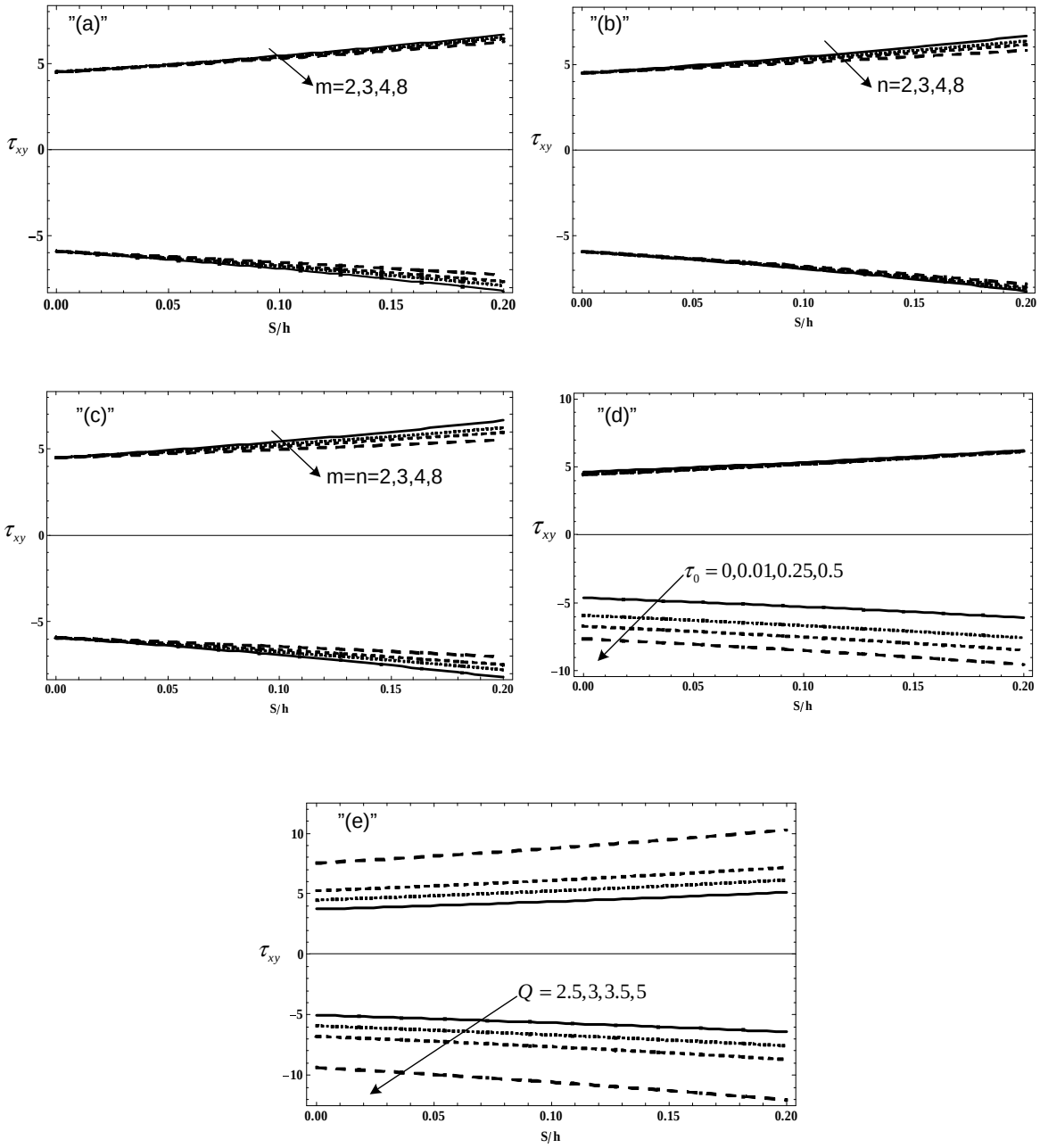

FIGURE 9. Variation of τ_{xy} with s/h at $x = 0.3$ and $\tau = 0.3$ for (a) $n = 2$, $\tau_0 = 0.1$, $Q = 3$, (b) $m = 2$, $\tau_0 = 0.1$, $Q = 3$, (c) $\tau_0 = 0.1$, $Q = 3$, (d) $m = 4$, $n = 3$, $Q = 3$, and (e) $m = 4$, $n = 3$, $\tau_0 = 0.1$.

5. **Conclusions**

Casson fluid model for blood flow through asymmetric mild stenosis artery has been analyzed. The effects of various flow parameters in the stenosed artery such as; shape parameters, stenosis length, stenosis size, yield stress, flow rate on the axial velocity, wall shear stresses, resistance

to flow (resistance impedance) and apparent viscosity at the walls are graphed and discussed in details. The present results are itemized as follows:

- The resistance impedance, λ, increases as the stenosis length, L_0/L, stenosis size, s/h, and Q increase. However, It decreases as the stenosis shape parameters (i.e. m and n) and τ_0 increase.
- The axial velocity flow, u, decreases when $\eta_n < y < 0$ while it increases for $0 < y < \eta_m$, both with an increase in m. However, u has an opposite behaviour on variation with n. Further, it increases as s/h, τ_0 and Q increase.
- The increasing rate of u for $\eta_n < y < 0$ in the upstream of the throat decreases with of m, whereas it increases with m in the downstream of the throat. However, the behaviour is opposite for $0 < y < \eta_m$ and in the influence of n. This velocity increases with an increase in τ_0 and Q and decreases with an increase stenosis size, s/h. Further, due to the rapid fall in the velocity profile from its peak value at the throat to approached value, one may anticipate the formulation of wake in the downstream of the throat.
- The apparent viscosity, μ, are smaller in the lower–region, $\eta_n < y < 0$, than those in the upper–region, $0 < y < \eta_m$. Further, μ increases as s/h, m, n and τ_0 increase while it decreases when Q increases. In addition, for various values of n, m, $m = n$, τ_0 and Q, the apparent viscosity gives highly value in the upper–region than itself in the lower–region.
- In the lower–region, the wall shear stresses, τ_{xy}, decreases in the upstream of the stenosis throat and then increases in the downstream. In addition, τ_{xy} decreases as s/h, τ_0, Q and s/h increase. Whereas in the upper–region, WSS follows the opposite tend. The flow characteristic decreases with increasing in the upstream of the throat but this property reverse in the downstream. In addition, τ_{xy} increases as s/h, τ_0, Q and s/h increase. τ_{xy} attains its maximum magnitude at the stenosis throat in the lower and upper regions.

In summary, it should be noted that some results for hydrodynamic fluid in [33] and [34] can be obtained as the special cases of the current analysis by choosing $n = m$ even though the Cartesian coordinates have been used. In addition, the current results are compatible with those obtained in [35] and [36].

Conflict of Interests

The authors declare that there is no conflict of interests.

REFERENCES

[1] C.G. Caro, T.J. Pedley, R.C. Sthroter, W.A Seed, The Mechanics of the Circulation, Oxford University Press, England (1978)

[2] M. Anand, K. Rajagopal, K.R. Rajagopal, A model for the formation and lysis blood clots, Pathophysiol Haemotasis 34 (2005), 109–120.

[3] M. Anand, K. Rajagopal, K.R. Rajagopal, A viscoelastic fluid model for describing the mechanics of a coarse ligated plasma clot, Theory Comput. Fluid Dyn. 20 (2006), 239–250.

[4] N. Misra, A. Sarkar, A. Srinivas, R. Kapusetti,Study of blood viscosity at low shear rate and its flow through viscoelastic tubes and ducts, Indian J. Phys. 86 (2012), 89–96.

[5] S. Noreen, T. Hayat, A. Alsaedi, M. Qasim, Mixed convection heat and mass transfer in peristaltic flow with chemical reaction and inclined magnetic field, Indian J. Phys. 87 (2012), 889–896.

[6] M.R. Gupta, R. Banerjee, L.K. Mandal, R. Bhar, H.C. Pant, M. Khan, Effect of viscosity and surface tension on the growth of RayleighTaylor instability and RichtmyerMeshkov instability induced two fluid interfacial nonlinear structure, Indian J. Phys. 86 (2012), 471–479.

[7] S. Kumari, A.K. Nirala, Study of light propagation in human and animal tissues by Monte Carlo simulation, Indian J. Phys. 86 (2012), 97–100.

[8] R. Bali, U. Awasthi, Effect of magnetic field on the resistance to blood flow through stenotic artery, Appl. Math. Comput. 188 (2007), 1635–1641.

[9] S. Chakravarthy, A. Datta, P.K. Mandal, Analysis of nonlinear blood flow in a stenosed flexible artery, Int. J. Eng. Sci. 33 (1995), 1821–1837.

[10] P. Chaturani, R.P. Samy, A study of non–Newtonian aspects of blood flow through stenosed arteries and its applications in arterial diseases, Biorhelogy 22 (1985), 521–531.

[11] S.A. Berger, L.D. Jou, Flows in stenotic vessels, Ann. Rev. Fluid Mech. 32 (2000), 347–382.

[12] S. Chien, Hemorheology in clinical medicine, Recent Adv. Cardiovascular Diseases 2 (1981), 21–26.

[13] C. Picart, J.M. Piau, H. Galliard, P. Carpentier, Human blood shear yield stress and its hematocrit dependence, J. Rheol. 1–12 (1998)

[14] S.E. Charm, G.S. Kurland, Blood Flow and Microcirculation, John Wiley & Sons, New York (1974)

[15] N.A. Casson, A flow equation for pigment-oil suspensions of the printing ink type. In C. C. Mill (Ed.), Rheology of disperse suspensions, Pergamon Press. New York (1959)

[16] S. Chakravarthy, P.K. Mandal, Unsteady flow of a two–layer blood stream past a tapered flexible artery under stonotic conditions, Comput. Methods Appl. Math. 4 (2004), 391–409.

[17] S.U. Siddiqui, S. Mishra, A study of modified Casson's fluid in modelled normal and stenotic capillary–tissue diffusion phenomena, Appl. Math. Comput. 189 (2007), 1048–1057.

[18] S. Sarifuddin, S. Chakravarty, P.K. Mandal, Effect of heat and mass transfer on non–Newtonian flow–links to atherosclerosis, Int. J. Heat Mass Transfer 52 (2009), 5719–5730.

[19] A. Javadzadegan, M. Esmaeili, S. Majidi, B. Fakhimghanbarzadeh, Pulsatile flow of viscous and viscoelastic fluids in constricted tubes, J. Mech. Sci. Tech. 23 (2009), 2456–2467.

[20] D.S. Sankar, U. Lee, Mathematical modelling of pulstatile flow of non–Newtonian fluid in stenosed arteries, Commun. Nonlinear Sci. Numer. Simulat. 14 (2009), 2971–2981.

[21] S. Nadeem, N.S. Akbar, A.A. Hendi, T. Hayat, Power law fluid model for blood flow through a tapered artery with a stenosis, Appl. Math. Comput. 217 (2011), 7108–7116.

[22] S. Bandyopadhyay, G.C. Layek, Numerical computation of pulsatile flow through a locally constricted channel, Commun. Nonlinear Sci. Numer. Simulat. 16 (2011), 252–265.

[23] R. Ellahi, S.U. Rahman, M.M. Gulzar, S. Nadeem, K. Vafai, A mathematical study of nonNewtonian micropolar fluid in arterial blood flow through composite stenosis, Appl. Math. Inf. Sci. 8 (2014), 1567–1573.

[24] S. Gupta, M. Gupta, A study of axial viscosity variation in an artery with mild stenosis: Bingham–Plastic fluid model, Int. J. Appl. Math. Mech. 10 (2014), 38–46.

[25] G. Awgichew, G. Radhakishnamacharya, B. Shireesha, Effect of slip condition on couple stress fluid flow in a channel with mild stenosis in the presence of uniform magnetic field, Appl. Appl. Math. 9 (2014), 54–67.

[26] N. Nandakumar, K.C. Sahu, M. Anand, Pulsatile flow of a shear– thinning model for blood through a two–dimensional stenosis channel, European J. Mech. B/Fluids 49 (2015), 29–35.

[27] V.P. Srivastava, R. Rastogi, Blood flow through a stenosed catheterized artery: Effects of hematocrit and stenosis shape, Comput. Math. Appl. 59 (2010), 1377–1385.

[28] D.F. Young, Effects of a time–dependent stenosis on flow through a tube, J. Eng. Ind. 90 (1968), 248–254.

[29] V.P. Srivastava, Blood flow through stenosed vessels with peripheral plasma layer and applications, Automedica 18 (2000), 271–300.

[30] R.B. Bird, W.E. Stewart, E.N. Lightfoot, Transport Phenomena, John Wiley & Sons, New York (1976)

[31] V.P. Srivastava, M. Saxena, Suspension model for blood flow through stenotic arteries with a cell–free plasma larger, Math. Biosci. 139 (1997), 79–102.

[32] B. Das, R.L. Batra, Non–Newtonian flow of blood in an arteriosclerotic blood vessel with rigid permeable walls, J. Theor. Biol. 175 (1995), 1–11.

[33] S.R. Shah, Analysis of non–Newtonian fluid flow in a stenosed artery, Int. J. Phys. Sci. 4 (2009), 663–671.

[34] S. Mishra, S.U. Siddiqui, A Mathematical model for flow and diffusion through stenotic capillary–tissue exchange system, e–J. Sci. & Tech. (e–JST) 6 (2011), 1–17.

[35] V.P. Srivastava, R. Rastogi, Blood flow through catheterized stenosed artery: Effects of hematocrit and stenosis shape, Comput. Math. Appl. 59 (2010), 1377–1385.

[36] Kh.S. Mekheimer, M.A. El Kot, The micropolar fluid model for blood flow through a tapered artery with a stenosis, Acta Mech. Sin. 24 (2008), 637–644.